



Evaluation of commercial 18650 and 26700 sodium-ion cells and comparison with well-established lithium-ion cells

Katharina Bischof^a, Vittorio Marangon^{b,c}, Michael Kasper^a, Aislím Aracil Regalado^a, Margret Wohlfahrt-Mehrens^{a,b}, Markus Hölzle^a, Dominic Bresser^{b,c,*}, Thomas Waldmann^{a,b,**}

^a Zentrum für Sonnenenergie- und Wasserstoff-Forschung Baden-Württemberg (ZSW), Helmholtzstrasse 8, Ulm, 89081, Germany

^b Helmholtz Institute Ulm (HIU), Helmholtzstrasse 11, Ulm, 89081, Germany

^c Karlsruhe Institute of Technology (KIT), P.O. Box 3640, Karlsruhe, 76021, Germany

ARTICLE INFO

Keywords:

Na-ion batteries
Li-ion batteries
Commercial cells
Heating
Specific energy

ABSTRACT

Recently, the first sodium-ion cells have been commercialized and have become available for consumers. Given, moreover, the exciting announcements by several producers of such battery cells, it is of great interest to analyze these first commercial cells in order to understand which materials are used and how these cells are designed. Herein, two types of commercially available sodium-ion battery cells (cylindrical 1.5 Ah 18650 and 3.5 Ah 26700 cells) are investigated regarding (i) their electrode chemistry, (ii) their thermal properties upon discharge as a function of the applied C rate, (iii) the available specific energy, and (iv) their cell impedance. The data are correlated with the electrode thickness and electrode area obtained from an *ex situ* (ante-mortem) analysis of the 18650 cells, and discussed in comparison with the performance metrics reported for commercial lithium-ion cells. This comparison reveals that the herein studied 18650 sodium-ion cells (hard carbon \parallel $\text{Na}_x\text{Ni}_y\text{Fe}_z\text{Mn}_{1-y-z}\text{O}_2$) provide a comparable or even higher specific energy ($\sim 128 \text{ Wh kg}^{-1}$) than that of graphite \parallel LiFePO_4 lithium-ion cells.

1. Introduction

The continuous improvement of lithium-ion batteries (LIBs) has enabled the widespread diffusion of portable electronic devices and (hybrid) electric vehicles (EVs) over the past three decades [1–3]. This tremendous success and the anticipated further increase in LIB sales [3], however, may cause shortages of the critical elements and compounds used in LIBs such as cobalt, copper, lithium, and graphite [4,5]. In view of these potential future limitations, sodium-ion batteries (SIBs), which can be built without using any of these elements and compounds, may represent a more sustainable alternative, in particular for stationary energy storage applications and light vehicles, for which the eventual energy density plays a less decisive role than the total cost and lifetime of the battery cells [6,7]. In fact, copper, used in LIBs as the anode current collector, can be replaced by aluminum, as aluminum does not alloy with sodium at low potentials in contrast to lithium [8]. Graphite as the currently most used LIB anode material has to be replaced by hard carbon, since sodium cations only intercalate to a very minor extent into

graphite [9–12]. Furthermore, it is possible to realize high-performance layered sodium transition metal oxides for the positive electrode that do not contain cobalt and only limited nickel concentrations [8,10,13,14]. All these advantages on the material side have triggered the development and very recent commercialization of SIBs along with several announcements of current LIB manufacturers to enter the production and commercialization of SIBs in the near future, targeting specific energy values of 120–160 Wh kg^{-1} at the cell level [15]. While these values are backed up by very reasonable estimations [7], first studies on commercialized and 18650 prototype SIBs reported excellent cycle life and rate capability as well as promising further improvement strategies for cells using either a layered transition metal oxide-based [16,17], a fluorophosphate-based [18–21] or a Prussian Blue analogue-based [22] cathode. However, these cells showed only rather limited specific energies of 43–97 Wh kg^{-1} [17,18,20–22]. In fact, one of these studies even revealed that there was still copper used as the current collector for the negative electrode in such commercial SIB cells [17]. These initial findings highlight the need for more data from commercial SIB cells to

* Corresponding author. Helmholtz Institute Ulm (HIU), Helmholtzstrasse 11, Ulm, 89081, Germany.

** Corresponding author. Zentrum für Sonnenenergie- und Wasserstoff-Forschung Baden-Württemberg (ZSW), Helmholtzstrasse 8, Ulm 89081, Germany.

E-mail addresses: dominic.bresser@kit.edu (D. Bresser), thomas.waldmann@zsw-bw.de (T. Waldmann).

understand their design philosophy and the interlink between battery design and battery performance.

Here, we report first insights into another very recently commercialized SIB cell comprising a hard carbon anode on an aluminum current collector and a cobalt-free layered sodium transition metal oxide cathode. Two different cell formats, i.e., 18650 (1.5 Ah) and 26700 (3.5 Ah) cells both operating at a nominal voltage of 3.0 V, are investigated concerning their specific energy, rate capability, thermal properties, and cell impedance. Additionally, an *ex situ* (ante-mortem) analysis of the electrode thicknesses and active material mass loadings is performed for the 18650 cells. These preliminary results are discussed in comparison with a variety of commercial LIBs in order to set the basis for a comprehensive analysis of commercial battery cells and cell formats.

2. Experimental

Two commercial 18650 cells with a nominal capacity of 1.5 Ah and one 26700 cell with a nominal capacity of 3.5 Ah from Selian Energy's battery brand HAKADI (China) were investigated. For both cell types, a voltage range between 1.5 V and 4.1 V and a cell impedance of ≤ 20 m Ω was specified, with maximum C rates of 1C and 3C during charge and discharge, respectively. All electrochemical tests were conducted using BaSyTec CTS and XCTS systems at room temperature (25 °C). Discharge rate capability tests within the specified voltage range were performed on one of the 18650 cells and the 26700 cell. These cells had a mass of 37.4 g (18650) and 84.2 g (26700). Constant current-constant voltage (CC-CV) charging at a C rate of C/2 and a CV cut-off current of C/20 was used for all charging steps. The C rates for the CC discharge steps were C/10, C/5, C/3, C/2, 1C, 2C, and 3C. Between the charge and discharge steps, there was a rest period of 1 h. To investigate the heating behavior during discharge as a function of the C rate applied, the temperature on the cell surface was measured during the tests by NTC-type temperature sensors. These sensors were taped at mid-height of the cells following previous investigations on cylindrical LIB cells, which indicated that the maximum temperature during discharge is reached at this position [23]. The cell impedances were determined in the fully charged state at 1 kHz using a Hioki 3554 battery tester. The specific energies were calculated from the capacity values obtained upon discharge to 1.5 V at a C rate of C/2 at 25 °C.

Another 18650 cell was disassembled under inert conditions in an Ar-filled glovebox ($[O_2] < 0.1$ ppm, $[H_2O] < 0.1$ ppm, MBraun) after CC discharge to the cut-off voltage of 1.5 V. The electrode and separator dimensions along with the electrode mass loadings were measured (see Table 1) and, subsequently, the electrodes were washed three times for 1 min each in dimethyl carbonate (DMC) and dried under vacuum for further analyses. The thickness of the double-side coated electrodes, current collectors (aluminum foil for both the cathode and anode), and the separator was determined using a micrometer gauge at ambient conditions. The morphological features of the electrodes retrieved from the 18650 cell were investigated via scanning electron microscopy (SEM) using a Zeiss LEO 1550 microscope operated with an accelerating voltage of 5 kV and energy-dispersive X-ray spectroscopy (EDX)

Table 1

Basic properties of the anode, cathode and separator of the 18650 cells. The thickness measurements indicate mean values of five measurements. d_{asc} is the sum of the thicknesses of the anode, cathode (both double-side coated including the current collector foil), and the two separators.

| | Anode | Cathode |
|--|-----------------------|------------------------|
| Coating loading (single-sided) | 9 mg cm ⁻² | 19 mg cm ⁻² |
| Coating thickness (single-sided) | ~89 μ m | ~63 μ m |
| Current collecting foil (Al) thickness | 12 μ m | 12 μ m |
| Coated electrode area | 775 cm ² | 716 cm ² |
| Tab number | 2 | 1 |
| Separator thickness | 13 μ m | |
| d_{asc} | 355 μ m | |

employing an X-ACT Cambridge Instrument linked to the electron microscope. Inductively coupled plasma optical emission spectroscopy (ICP-OES) was performed for the cathode coating after scratching the coating layer from the electrode via a Spectro Arcos system (Spectro Analytical Instruments).

3. Results and discussion

Fig. 1 shows the SEM-EDX data acquired for the surface of the cathode and anode retrieved from the 18650 SIB cell. The SEM micrographs recorded for the cathode reveal secondary active material particles with a diameter ranging from 2 to 10 μ m (Fig. 1a), which are composed of primary particles with a size of a few hundred nanometers and interconnected through a binder/conductive-carbon network (Fig. 1b). The EDX analysis (Fig. 1c) displays the presence of Na, Ni, Mn, Fe, and O (Fig. 1d–h), indicating that the general composition of the active material is Na_xNi_yFe_zMn_{1-y-z}O₂ (NFM), as suggested by both EDX and ICP-OES (Table 2). Interestingly, EDX and ICP-OES show in Table 2 a sodium content of 0.80 and 0.88, respectively. This slight discrepancy is likely resulting from the different nature of these two methods – with EDX being a more surface-sensitive technique and ICP-OES being a bulk analysis technique – in combination with the common experimental error of both techniques. The SEM micrographs acquired for the anode exhibit micrometric active material particles, which are surrounded by nanometric binder/conductive-carbon domains (Fig. 1i–j). The EDX mapping recorded for an SEM micrograph at a lower magnification (Fig. 1k) reveals the expected presence of C and some traces of O and Na, most likely resulting from the initial electrolyte decomposition during the formation cycles conducted by the manufacturer (Fig. 1l and m).

Fig. 2a shows the discharge voltage curves of the two commercial SIB cells vs. the normalized capacity at C rates ranging from C/10 to 3C. The shape of the discharge voltage profiles of both the 18650 and 26700 cells matches very well the characteristic signature of SIBs comprising NFM cathodes and hard carbon anodes [24], confirming the conclusions from the EDX data depicted in Fig. 1 and that both kinds of cells are comprising most likely the same cell chemistry. In addition, it is observed that both cells exhibit a very good rate capability, as demonstrated by the limited capacity decay when increasing the C rate from C/10 (100% normalized capacity) to 3C (~95% of normalized capacity). This is in good agreement with the performance results reported by Zhou et al. [16] for a 26650-type SIB cell with a copper-containing layered oxide cathode and a hard carbon anode, which still provided 90% of the discharge capacity at C/5 during discharge at a high C rate of 10C. Notably, the 26700 cell of the present study shows a more pronounced increase in polarization at high C rates compared to the 18650 cell, which might be originating simply from the different cell design and/or a different electrode coating thickness and/or a different mass loading.

Fig. 2b depicts the temperature recorded at the surface (mid height of the cylindrical cells) of the 18650 and the 26700 SIB cells. Higher discharge rates cause a steeper and stronger temperature rise. Consequently, higher maximum temperatures (T_{max}) are reached at the end of discharge. This trend is consistent with LIB cells [23,25–27]. The maximum temperatures T_{max} are plotted as a function of the discharge rate in Fig. 2c. For both the 18650 and the 26700 SIB cells, T_{max} correlates linearly with the C rate ($R^2 \geq 0.998$), which is, again, consistent with previous studies on LIB cells [23,25,26,28,29]. The slopes from the linear fits in Fig. 2c are very helpful to describe the heating behavior as a result of the current flow. In fact, for LIB cells, it is known that the $T_{max}/(C \text{ rate})$ ratio is influenced by the cell volume to surface ratio, which has an important impact on the heat dissipation properties of the cell [28]. For LIB cells with different cell geometries, it was found that higher surface to volume ratios lead to higher $T_{max}/(C \text{ rate})$ values [28]. Therefore, the steeper slope of the linear fit of the data recorded for the 26700 cell and the concomitant higher $T_{max}/(C \text{ rate})$ value compared to the 18650 cell, reflecting a stronger increase of the cell temperature at

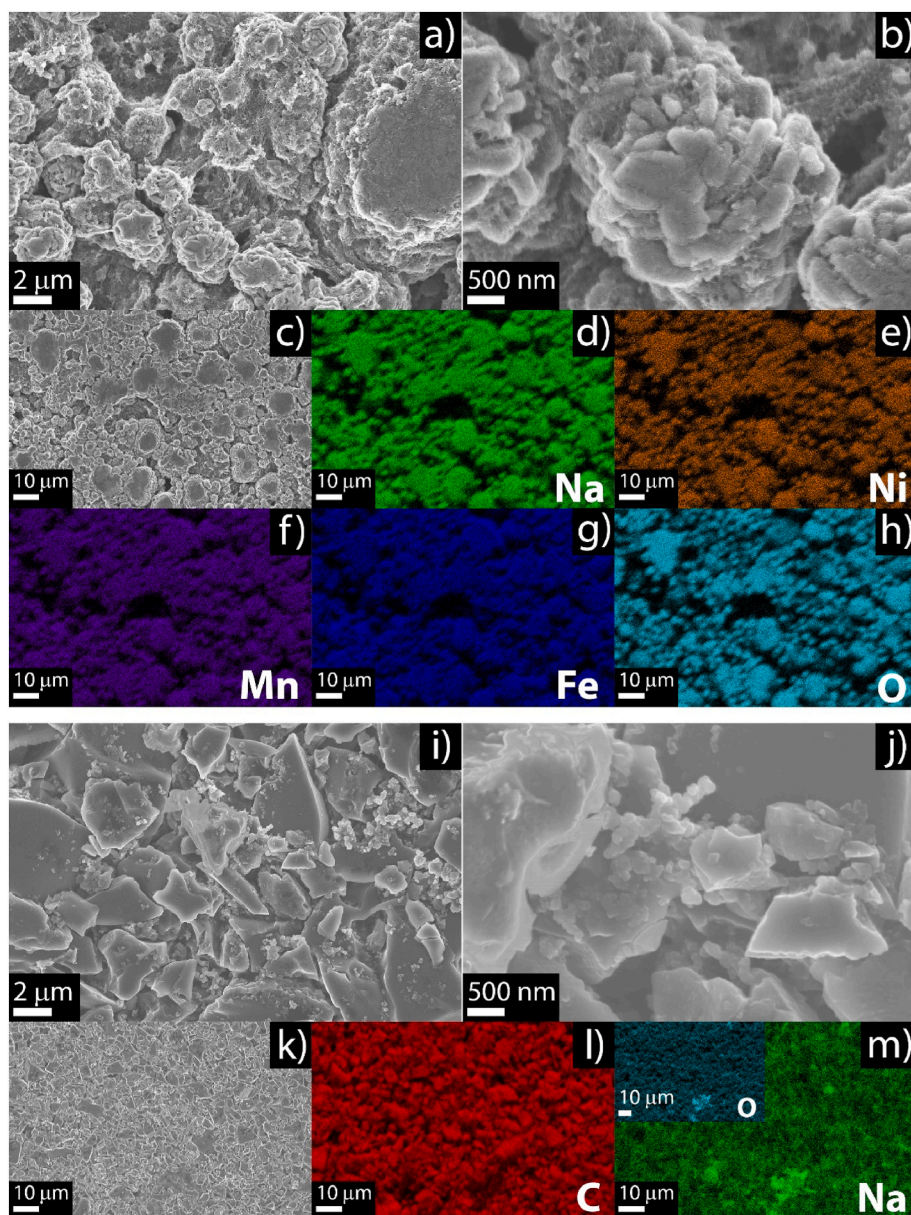


Fig. 1. SEM-EDX analysis performed on the cathode and anode retrieved from the 18650 SIB cell: a-c) SEM micrographs of the cathode and d-h) the corresponding EDX elemental maps for d) Na, e) Ni, f) Mn, g) Fe, and h) O; i-k) SEM micrographs of the anode and l-m) the corresponding EDX elemental maps for l) C, m) Na, and O in the inset of m).

Table 2

EDX and ICP-OES elemental analysis carried out on the cathode retrieved from the 18650 SIB commercial cell (see the Experimental section for details concerning the sample preparation). The results are reported in atomic and mass percentages for the EDX and ICP-OES data, respectively, as well as the stoichiometric coefficient for both methods.

| Element (cathode) | EDX (At. %) | EDX (stoich.) | ICP-OES (mass %, ± 10 %) | ICP-OES (stoich.) |
|-------------------|-------------|---------------|------------------------------|-------------------|
| Na | 12.1 | 0.80 | 16.9 | 0.88 |
| Ni | 4.8 | 0.32 | 16.6 | 0.34 |
| Mn | 5.1 | 0.34 | 14.9 | 0.33 |
| Fe | 5.2 | 0.34 | 15.2 | 0.33 |

elevated discharge rates for the 26700 cell, most likely result from the higher surface to volume ratio of the 26700 cell. Another important factor influencing $T_{\max}/(C \text{ rate})$ is d_{asc} , which is the sum of the thicknesses of the anode and cathode (both double-side coated and including

the current collector foil) as well as the two separators in the jellyroll of cylindrical cells [23]. We note that a tabless design can decrease $T_{\max}/(C \text{ rate})$ drastically [29]. However, this can be neglected in the present paper, since none of the cells discussed has such a design. Hence, the $T_{\max}/(C \text{ rate})$ values for the SIB cells are set into comparison with 11 types of commercial or pilot-line built LIB cells from Ref. [28] in Fig. 3a. The 18650 SIB cell ($d_{\text{asc}} = 355 \mu\text{m}$) shows a similar heating behavior compared to an 18650 LIB cell ($d_{\text{asc}} = 341 \mu\text{m}$). Besides the slightly higher $T_{\max}/(C \text{ rate})$ value for this LIB cell in comparison to the SIB cell, the values of both cell types are comparable. The slightly higher value for the LIB cell might originate from minor cell design differences, e.g. a different number of tabs. In the case of the 26700 cell, its increased volume to surface ratio compared to the 18650 cell likely contributes to its increased $T_{\max}/(C \text{ rate})$ ratio, as discussed above.

Fig. 3b shows $T_{\max}/(C \text{ rate})$ as a function of d_{asc} for five types of 18650 LIB cells and the 18650 SIB cell. Higher d_{asc} values tend to result in a higher dependence of T_{\max} on the discharge C rate at a constant

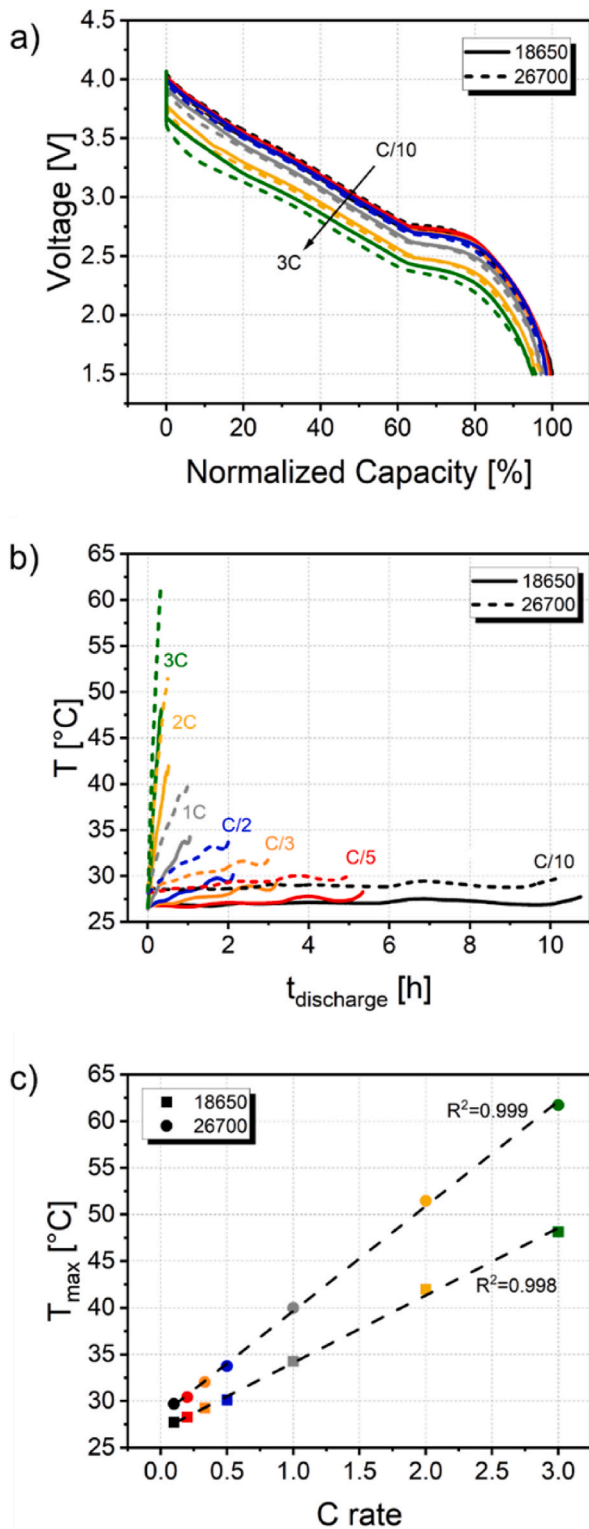


Fig. 2. a) Comparison of the voltage profiles during discharge of the 18650 SIB cell (solid lines) and the 26700 SIB cell (dashed lines). b) Direct comparison of the temperature rise on the surface of these cells during discharge at different C rates. c) Maximum temperatures from (b) (squares: 18650; circles: 26700) as a function of the C rate during discharge. The dashed lines are linear fits. The general color coding in a-c) is: black: C/10, red: C/5, orange: C/3, blue: C/2, grey: 1C, yellow: 2C, and green: 3C. (For interpretation of the references to color in this figure legend, the reader is referred to the Web version of this article.)

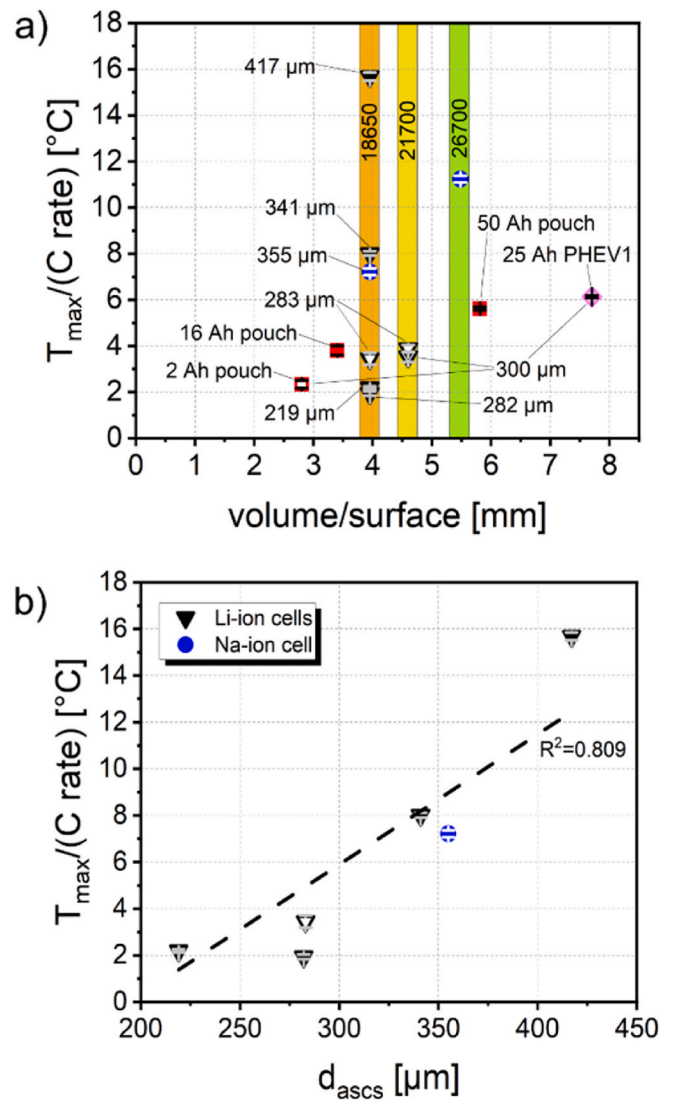


Fig. 3. a) Plot of the $T_{\max}/(C \text{ rate})$ ratio, as obtained from Fig. 2c, vs. the volume to surface ratio for the 18650 and 26700 SIB cells investigated in this study (blue circles) in comparison with data from LIB cells as reported in the literature: Commercial pouch cells (filled red squares) with 16 Ah [23] and 50 Ah [27], pilot-line built pouch cells (empty red squares) with 2 Ah [28], commercial 18650 cells (filled black triangles) [23], pilot-line built 18650 [30] and 21700 [28,30] cells (empty black triangles), and pilot-line built PHEV1 cells with 25 Ah [28] (empty pink rhombus). The given values in μm correspond to the thicknesses d_{asc} (sum of the thicknesses of anode, cathode and two separators). b) Comparison of the $T_{\max}/(C \text{ rate})$ ratio as a function of d_{asc} for the 18650 LIB cells from (a) (black triangles) with the 18650 SIB cell investigated in this study (blue circle). The dashed line is a linear fit of the data reported for the LIB cells with a slope of $0.056 \pm 0.016 \text{ } ^\circ\text{C } \mu\text{m}^{-1}$ ($R^2 = 0.809$). It is worth noting that the plots contain error bars which are, however, very small. (For interpretation of the references to color in this figure legend, the reader is referred to the Web version of this article.)

surface to volume ratio, and the heating behavior of the 18650 SIB cell fits well into this trend. Overall, the $T_{\max}/(C \text{ rate})$ values determined for the two different SIB cells studied herein are in a similar range as the values that have been reported earlier for commercial and pilot-scale LIB cells.

Fig. 4a displays a comparison of the specific energy at cell level as a function of the single-sided anode coating thickness. This plot enables a comparison of high-power and high-energy cells of different type. For LIB cells with graphite anodes, the data correlate linearly ($R^2 = 0.997$) [31]. We note that this correlation includes data from eight types of

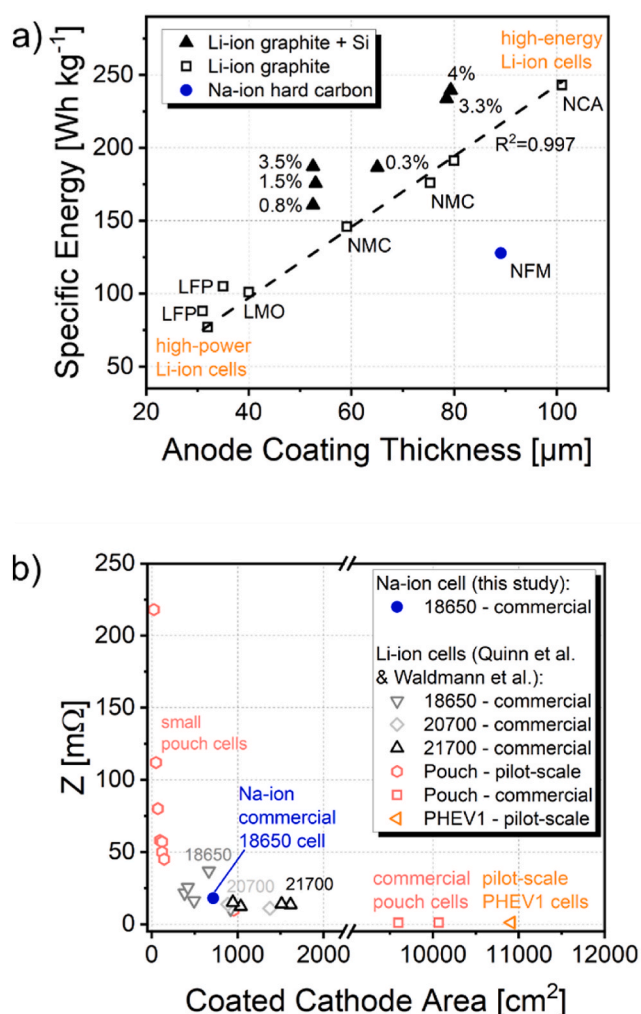


Fig. 4. a) Correlation of the specific energy with the single-sided anode coating thickness for commercial cylindrical LIB cells containing either pure graphite (empty squares) or Si/graphite composites (black triangles, Si content given in %) as the anode active material and comparison with the data of the 18650 SIB cell (blue circle) investigated herein. The specific energy was calculated from the discharge capacity obtained at C/2 for all cell types. b) Cell impedance at 1 kHz as a function of the coated cathode area for the 18650 SIB cell and comparison with the data reported for commercial and pilot-scale LIB cells [28,32]. (For interpretation of the references to color in this figure legend, the reader is referred to the Web version of this article.)

commercial LIB cells from different manufacturers with different cell chemistries, electrode porosities, and different cell dimensions (18650, 20700, and 21700) [32]. These differences lead to some scattering around the linear fit, but the overall trend appears generally applicable, as also indicated by the high fitting coefficient [31,32]. This correlation between the specific energy and anode coating thickness is related to the fact that higher anode coating thicknesses lead to an improved ratio of active to inactive materials and therefore an increased specific energy at cell level [31,32]. For LIB cells with Si/graphite anodes, the data points are located above the dashed line for the linear trend owing to the higher specific capacity of such composites compared to neat graphite anodes and the resulting increase in specific energy [31,33].

Differently, the data point for the 18650 SIB cell lies well below the dashed line, reflecting that the SIB cell provides a lower specific energy than a LIB cell with a graphite anode having the same coating thickness, presumably owing to, amongst others, the lower density and specific capacity of commonly used hard carbons (ca. 300 mAh g⁻¹ [34,35])

compared to graphite (ca. 360 mAh g⁻¹ [33]) as well as a lower packing density of the hard carbon electrodes compared to graphite electrodes [36,37]. In fact, a lower electrode density, i.e., a higher electrode porosity, leads to a greater amount of electrolyte needed to fully fill all the pores, which adds to a lower specific energy. The effect of the cathode chemistry is well reflected by the increasing trend from LiFePO₄ (LFP) and LiMn₂O₄ (LMO) to LiNi_{1-x-y}Mn_xCo_yO₂ (NMC) and, finally, LiNi_{1-x-y}Co_xAl_yO₂ (NCA), i.e., from LIB cells that are more designed for high power applications with thinner anodes towards LIB cells for high energy applications with thicker anodes. Remarkably, the 18650 SIB cell (128 Wh kg⁻¹) and the 26700 SIB cell (124 Wh kg⁻¹) provide specific energies at C/2 that are at least comparable to the tested 18650 LIB cells with an LFP cathode (88–105 Wh kg⁻¹) optimized for high power applications, rendering such comparison suitable with regard to the remarkable rate capability demonstrated for 18650 SIB prototype cells and commercial 26650 SIB cells [16,18,21], even though the SIB cells of the present study have not been declared by the manufacturer to be specifically optimized for either high power or high energy applications. In fact, one major difference is the significantly greater anode coating thickness (~89 μm) of the 18650 SIB cell compared to the LFP-based LIB cells (31–35 μm) as already discussed above. We might also note that the SIB cells studied herein provide a higher specific energy than a recent report on a hard carbon | Na₃V₂(PO₄)₂F₃ 18650 SIB prototype cell with about 70 Wh kg⁻¹ [18].

To complete this comparison of the commercial and pilot-scale LIB and commercial SIB cells, we determined the impedance of the two SIB cells. A main influence on the cell impedance of LIB cells is the coated cathode area [32]. The cell impedance depends inversely on the cathode area, comparable to the overall resistance of resistors connected in parallel [32]. This trend for LIB cells with a variety of different cathodes [32] is depicted in Fig. 4b for impedance measurements at 1 kHz, enabling a comparison of different cell types. Small LIB pouch cells consequently show the highest impedances, followed by 18650, 20700, and 21700 cylindrical cells, while large pouch and prismatic cells show the lowest impedances. Other minor influences are the tab design [29] and the cell chemistry, leading to (minor) deviations from the general trend. In fact, also the impedance of the 18650-type SIB cell (18.6 mΩ) and the 26700 SIB cell (15.4 mΩ) at 1 kHz fit well into this general trend, highlighting that these trends are applicable also to SIBs and, thus, enabling a rather straightforward comparison of these different cell chemistries (just like for different LIB cell chemistries).

4. Conclusions

The first results of the evaluation of two types of commercially available SIBs (18650 and 26700) are presented and compared to a variety of commercial and pilot-scale LIBs. As confirmed by EDX and ICP-OES analysis and the shape of the discharge profile, the SIB cells comprise a hard carbon anode and a Na_xNi_yFe_zMn_{1-y-z}O₂ (NFM) cathode. The maximum temperature reached on the cell surface correlates linearly with the C rate applied upon discharge for both cell formats, and the values for the T_{max}/(C rate) ratio are in a similar range as those reported earlier for different LIB cells, indicating a comparable heating behavior for both battery technologies. The SIBs provide a specific energy of more than 120 Wh kg⁻¹, which is higher than the specific energy of the tested LFP-based LIBs that have been designed for high power applications owing to the substantially thicker anode coating in the case of the SIBs. Besides, also the cell impedances of the SIB cells measured at 1 kHz are in a comparable range as the values that have been reported earlier for cylindrical LIB cells.

We may anticipate that these results will provide a starting point for a comprehensive evaluation of the performance metrics of SIBs and contribute to a meaningful comparison with commercial LIBs in order to help selecting the appropriate battery chemistry for a given application. In fact, the SIB cells studied herein provide competitive performance metrics, opening up a greater choice for consumers in the future.

CRedit authorship contribution statement

Katharina Bischof: Writing – original draft, Methodology, Investigation, Formal analysis, Data curation, Conceptualization. **Vittorio Marangon:** Writing – review & editing, Methodology, Investigation, Formal analysis, Data curation. **Michael Kasper:** Investigation, Formal analysis, Data curation. **Aislim Aracil Regalado:** Investigation, Formal analysis, Data curation. **Margret Wohlfahrt-Mehrens:** Writing – review & editing, Supervision, Funding acquisition. **Markus Hölzle:** Writing – review & editing, Supervision, Funding acquisition. **Dominic Bresser:** Writing – review & editing, Supervision, Methodology, Funding acquisition, Conceptualization. **Thomas Waldmann:** Writing – review & editing, Supervision, Methodology, Funding acquisition, Conceptualization.

Declaration of competing interest

The authors declare that they have no known competing financial interests or personal relationships that could have appeared to influence the work reported in this paper.

Data availability

Data will be made available on request.

Acknowledgment

K.B., M.K., A.A.R., M.W.-M, M.H., and T.W. gratefully acknowledge ZSW for financial support. V.M. and D.B. would like to acknowledge financial support from the Ministry of Economics, Labor and Tourism in Baden-Wuerttemberg (Ministerium für Wirtschaft, Arbeit und Tourismus Baden-Württemberg) within the frame of the PRONTO project (WM34-42-57/19) as well as from the Helmholtz Association.

References

- Armand, J.-M. Tarascon, Nature 451 (2008) 652–657, <https://doi.org/10.1038/451652a>.
- Armand, P. Axmann, D. Bresser, M. Copley, K. Edström, C. Ekberg, D. Guyomard, B. Lestriez, P. Novák, M. Petrankova, W. Porcher, S. Trabesinger, M. Wohlfahrt-Mehrens, H. Zhang, J. Power Sources 479 (2020) 228708, <https://doi.org/10.1016/j.jpowsour.2020.228708>.
- Marinero, D. Bresser, E. Beyer, P. Faguy, K. Hosoi, H. Li, J. Sakovica, K. Amine, M. Wohlfahrt-Mehrens, S. Passerini, J. Power Sources 459 (2020) 228073, <https://doi.org/10.1016/j.jpowsour.2020.228073>.
- Calvo, A. Valero, Environmental Development 41 (2022) 100640, <https://doi.org/10.1016/j.envdev.2021.100640>.
- Olivetti, G. Ceder, G.G. Gaustad, X. Fu, Joule 1 (2017) 229–243, <https://doi.org/10.1016/j.joule.2017.08.019>.
- Vaalma, D. Buchholz, M. Weil, S. Passerini, Nat. Rev. Mater. 3 (2018) 1–11, <https://doi.org/10.1038/natrevmats.2018.13>.
- Hasa, S. Mariyappan, D. Saurel, P. Adelhelm, A.Y. Kopsosov, C. Masquelier, L. Croguennec, M. Casas-Cabanas, J. Power Sources 482 (2021) 228872, <https://doi.org/10.1016/j.jpowsour.2020.228872>.
- J.-Y. Hwang, S.-T. Myung, Y.-K. Sun, Chem. Soc. Rev. 46 (2017) 3529–3614, <https://doi.org/10.1039/c6cs00776g>.
- Y. Cao, L. Xiao, M.L. Sushko, W. Wang, B. Schwenzer, J. Xiao, Z. Nie, L.V. Saraf, Z. Yang, J. Liu, Nano Lett. 12 (2012) 3783–3787, <https://doi.org/10.1021/nl3016957>.
- D.A. Stevens, J.R. Dahn, J. Electrochem. Soc. 148 (2001) A803, <https://doi.org/10.1149/1.1379565>.
- A. Metrod, D. Guerdard, D. Billaud, A. Herold, Synth. Met. 1 (1980) 363–369, [https://doi.org/10.1016/0379-6779\(80\)90071-5](https://doi.org/10.1016/0379-6779(80)90071-5).
- P. Ge, M. Foulletier, Solid State Ionics 28-30 (1988) 1172–1175, [https://doi.org/10.1016/0167-2738\(88\)90351-7](https://doi.org/10.1016/0167-2738(88)90351-7).
- J. Zhang, W. Wang, W. Wang, S. Wang, B. Li, ACS Appl. Mater. Interfaces 11 (2019) 22051–22066, <https://doi.org/10.1021/acsami.9b03937>.
- Z. Cai, S. Wang, M. Tao, Q. Li, H. Mei, Z. Ahsan, Y. Ma, Z. Yu, G. Song, W. Yang, C. Wen, T.-F. Yi, J. Energy Storage 74 (2023) 109391, <https://doi.org/10.1016/j.est.2023.109391>.
- A. Rudola, R. Sayers, C.J. Wright, J. Barker, Nat. Energy 8 (2023) 215–218, <https://doi.org/10.1038/s41560-023-01215-w>.
- Q. Zhou, Y. Li, F. Tang, K. Li, X. Rong, Y. Lu, L. Chen, Y.-S. Hu, Chin. Phys. Lett. 38 (2021) 76501, <https://doi.org/10.1088/0256-307X/38/7/076501>.
- H. Laufen, S. Klick, H. Dittler, K.L. Quade, A. Mikitisin, A. Blömeke, M.F. Schütte, D. Wasylowski, M. Sonnet, L. Henrich, A. Schwedt, G.K. Stahl, F. Ringbeck, J. Mayer, D.U. Sauer, Extensive Multi-Method Characterization of a Commercial 1.2 Ah 18650 Sodium-Ion Battery Cell. <https://ssrn.com/abstract=45422132023>.
- M. He, A.E. Mejdoubi, D. Chartouni, M. Morcrette, P. Troendle, R. Castiglioni, J. Power Sources 588 (2023) 233741, <https://doi.org/10.1016/j.jpowsour.2023.233741>.
- P. Desai, J. Forero-Saboya, V. Meunier, G. Rousse, M. Deschamps, A.M. Abakumov, J.-M. Tarascon, S. Mariyappan, Energy Storage Mater. 57 (2023) 102–117, <https://doi.org/10.1016/j.ensm.2023.02.004>.
- L. Nguyen, P.S. Camacho, J. Fondard, D. Carlier, L. Croguennec, M.R. Palacin, A. Ponrouch, C. Courrèges, R. Dedryvère, K. Trad, C. Jordy, S. Genies, Y. Reynier, L. Simonin, J. Power Sources 529 (2022) 231253, <https://doi.org/10.1016/j.jpowsour.2022.231253>.
- T. Broux, F. Fauth, N. Hall, Y. Chatillon, M. Bianchini, T. Bamine, J.-B. Leriche, E. Suard, D. Carlier, Y. Reynier, L. Simonin, C. Masquelier, L. Croguennec, Small Methods 3 (2019) 1800215, <https://doi.org/10.1002/smt.201800215>.
- L.U. Subasinghe, G. Satyanarayana Reddy, A. Rudola, P. Balaya, J. Electrochem. Soc. 167 (2020) 110504, <https://doi.org/10.1149/1945-7111/ab9ee9>.
- T. Waldmann, G. Bisle, B.-I. Hogg, S. Stumpp, M.A. Danzer, M. Kasper, P. Axmann, M. Wohlfahrt-Mehrens, J. Electrochem. Soc. 162 (2015) A921–A927, <https://doi.org/10.1149/2.0561506jes>.
- Q. Zhang, Z. Shi, Energy & Environ. Materials 6 (2023), <https://doi.org/10.1002/eem2.12523>.
- T. Waldmann, M. Wohlfahrt-Mehrens, ECS Electrochemistry Letters 4 (2014) A1–A3, <https://doi.org/10.1149/2.0031501eel>.
- T. Waldmann, G. Geramifard, M. Wohlfahrt-Mehrens, J. Energy Storage 5 (2016) 163–168, <https://doi.org/10.1016/j.est.2015.12.007>.
- C. Veth, D. Dragicevic, C. Merten, J. Power Sources 267 (2014) 760–769, <https://doi.org/10.1016/j.jpowsour.2014.05.139>.
- T. Waldmann, S. Rössler, M. Blessing, R. Schäfer, R.-G. Scurtu, W. Braunwarth, M. Wohlfahrt-Mehrens, J. Electrochem. Soc. 168 (2021) 90519, <https://doi.org/10.1149/1945-7111/ac208c>.
- T. Waldmann, R.-G. Scurtu, D. Brändle, M. Wohlfahrt-Mehrens, Energy Tech 11 (2023) 2200583, <https://doi.org/10.1002/ente.202200583>.
- T. Waldmann, R.-G. Scurtu, K. Richter, M. Wohlfahrt-Mehrens, J. Power Sources 472 (2020) 228614, <https://doi.org/10.1016/j.jpowsour.2020.228614>.
- M. Flügel, K. Richter, M. Wohlfahrt-Mehrens, T. Waldmann, J. Electrochem. Soc. 169 (2022) 50533, <https://doi.org/10.1149/1945-7111/ac70af>.
- J.B. Quinn, T. Waldmann, K. Richter, M. Kasper, M. Wohlfahrt-Mehrens, J. Electrochem. Soc. 165 (2018) A3284–A3291, <https://doi.org/10.1149/2.0281814jes>.
- J. Asenbauer, T. Eisenmann, M. Kuenzel, A. Kazzazi, Z. Chen, D. Bresser, Sustain. Energy Fuels 4 (2020) 5387–5416, <https://doi.org/10.1039/D0SE00175A>.
- D.A. Stevens, J.R. Dahn, J. Electrochem. Soc. 147 (2000) 1271, <https://doi.org/10.1149/1.1393348>.
- W. Shao, H. Shi, X. Jian, Z.-S. Wu, F. Hu, Adv. Energy and Sustain. Res. 3 (2022), <https://doi.org/10.1002/aesr.202200009>.
- L. Xie, C. Tang, Z. Bi, M. Song, Y. Fan, C. Yan, X. Li, F. Su, Q. Zhang, C. Chen, Adv. Energy Mater. 11 (2021) 2101650, <https://doi.org/10.1002/aenm.202101650>.
- A. Rudola, C.J. Wright, J. Barker, J. Electrochem. Soc. 168 (2021) 110534, <https://doi.org/10.1149/1945-7111/ac377a>.